ELSEVIER

Journal of Petroleum Science and Engineering 25 (2000) 59–77

JOURNAL OF PETROLEUM SCIENCE & ENGINEERING

www.elsevier.nl/locate/jpetscieng

# Lossy transmission line model of hydrofractured well dynamics

Tadeusz W. Patzek [a,b,*], Asoke De [b]

[a] *Department of Materials Science and Mineral Engineering, University of California at Berkeley, Berkeley, CA 94720, USA*
[b] *Earth Sciences Division, Lawrence Berkeley National Laboratory, Berkeley, CA 94720, USA*

Received 5 January 1999 ; accepted 8 October 1999

**Abstract**

The real-time detection of hydrofracture growth is crucial to the successful operation of water, $CO_2$ or steam injection wells in low-permeability reservoirs and to the prevention of subsidence and well failure. In this paper, we describe propagation of very low frequency (1–10 to 100 Hz) Stoneley waves in a fluid-filled wellbore and their interactions with the fundamental wave mode in a vertical hydrofracture. We demonstrate that Stoneley-wave loses energy to the fracture and the energy transfer from the wellbore to the fracture opening is most efficient in soft rocks. We conclude that placing the wave source and receivers beneath the injection packer provides the most efficient means of hydrofracture monitoring. We then present the lossy transmission line model of wellbore and fracture for the detection and characterization of fracture state and volume. We show that this model captures the wellbore and fracture geometry, the physical properties of injected fluid and the wellbore-fracture system dynamics. The model is then compared with experimentally measured well responses. The simulated responses are in good agreement with published experimental data from several water injection wells with depths ranging from 1000 ft to 9000 ft. Hence, we conclude that the transmission line model of water injectors adequately captures wellbore and fracture dynamics. Using an extensive data set for the South Belridge Diatomite waterfloods, we demonstrate that even for very shallow wells the fracture size and state can be adequately recognized at wellhead. Finally, we simulate the effects of hydrofracture extension on the transient response to a pulse signal generated at wellhead. We show that hydrofracture extensions can indeed be detected by monitoring the wellhead pressure at sufficiently low frequencies. 

*Keywords:* Hydrofracture extension; Hydrofracture monitoring; Hydraulic impedance analysis; Electrical transmission line model; Stoneley wave propagation

## 1. Introduction

Optimal performance of injection wells requires maximization of fluid injection and wellbore lifetime, subject to minimization of reservoir damage. Maximization of fluid injection results in, albeit inadvertent, extension of existing hydrofractures and naturally occurring fractures in the reservoir (e.g., Patzek and Silin, 1998). While large hydrofractures do dramatically improve oilfield profitability, uncontrolled extensions of injection fractures can lead to premature water, $CO_2$ or steam breakthrough at the producers, as well as to significant reservoir damage,

* Corresponding author. Department of Materials Science and Mineral Engineering, University of California at Berkeley, Berkeley, CA 94720, USA. Fax: +1-510-642-3805.
*E-mail address:* patzek@patzek.berkeley.edu (T.W. Patzek).

0920-4105/00/$ - see front matter 
PII: S0920-4105(99)00055-8

and can result in greatly impaired volumetric sweep. In addition, even a slight positive deviation from the optimal operating pressure may lead to catastrophic fracturing and well failure (Patzek, 1992). It is, therefore, essential to understand the response of the fractured formation to applied stresses and to identify the conditions that might lead to its catastrophic failure. Determination of these conditions through trial-and-error in real injectors is risky at best because it leads ultimately to wellbore failure.

In order to control reservoir damage effectively, we need a real-time ''observer'' of state of injection fractures. Since direct observation of such fractures is impossible, we need an indirect method. Active and passive seismic analysis can lead to an accurate characterization of fractured reservoirs (Vinegar et al., 1992; Winterstein, 1992; Ilderton et al., 1996; De et al., 1997), but it is rather expensive. In the eighties, Holzhausen and coworkers (Holzhausen and Gooch, 1985; Holzhausen and Egan, 1986; Holzhausen et al., 1989) introduced an inexpensive hydraulic impedance analysis to determine the fracture closure pressures and dimensions.

In contrast to classical well-testing techniques, hydraulic impedance is truly ''transient.'' It is a study of wave propagation and reflection. Inertial forces are accounted for by invoking the principle of momentum conservation. This principle, along with that of mass conservation, forms the basis of the study of oscillatory pressure and flow in wells and other conduits (Wylie and Streeter, 1978).

Hydraulic impedance testing involves the following. A short-duration pressure pulse is generated at wellhead in a fluid injector. Thus created pressure wave travels below the speed of sound in the wellbore fluid. Some of it enters the fracture through perforations; the remainder travels down to the bottom of the well. The pressure wave reaching the fracture mouth is partially reflected from an open fracture, depending on the fracture impedance, and the rest is transmitted through the fracture to the fracture tip, where it is again reflected. The fracture impedance is a function of its dimensions and the fluid and rock properties. In addition, the wave reflected from the well bottom travels to the fracture and to the wellhead. Because of energy leaks to the fluid-filled earth, the wellbore pressure waves are continually attenuated. The transient pressure measured at wellhead as a function of time results from the interference of all pressure waves reaching the wellhead at any instant of time.

The key to successful estimation of fracture characteristics from the transient response data is a model that captures the wellbore-fracture dynamics. In their analyses of transient responses, Holzhauzen and coworkers assumed no energy losses in the wellbore. While this greatly simplifies the analysis, it may also result in unacceptable errors in interpretation of experimental data. In addition, Holzhausen et al. modeled fracture as lumped capacitance and resistance in series, estimated by trial-and-error. Fracture capacitance was defined as the derivative of the fracture volume with respect to the hydraulic head. The fracture geometry was estimated from its capacitance using Sneddon's relationship between internal pressure and opening of an oblate-ellipsoidal fracture in an infinite elastic medium. Ashour and Yew (1996) extended this approach and presented a method of estimating fracture dimensions from wellhead data using inverse Fourier transform. Recent, not scaled, laboratory experiments by Paige et al. (1995) demonstrated that the pressure wave might indeed travel to the fracture tip. The reflected wave from the tip of the fracture can be detected at the wellhead, thereby providing a way of measuring the fracture length.

The goal of our research is to develop a model-based ''observer'' of hydrofracture growth and to use it to optimize water, $CO_2$ and steam injection in low permeability rocks. The observer is expected to provide a dynamic estimate of the dimensions and the state of hydrofractures from repeated hydraulic impedance tests. This information will then be used by a suitable control algorithm to maximize cumulative fluid injection and minimize reservoir damage (Patzek and Silin, 1998). The objectives of this paper are to demonstrate that (1) the proposed observer will actually work in a soft rock and (2) a lossy transmission line network model adequately captures the dynamic response of wellbore-fracture systems.

## 2. Wave propagation in a well with a vertical hydrofracture

Consider a cased and cemented fluid injection well with a vertical hydrofracture. Fluid is injected

through central tubing, which ends with a packer just above the perforated and hydrofractured interval (cf. Fig. 7). Through mechanical centralizers, tubing is weakly coupled with casing and the fluid-filled, soft earth. Stronger coupling with the earth exists through casing across the perforated interval. A cylindrical layer of cement between casing and the earth has the effect of stiffening the soft earth, decreasing casing compliance and energy leaks.

Periodically, fluid injection is stopped and a low-frequency (1–10 to 100 Hz) pulse is generated at the wellhead. This pulse is transmitted as a Stoneley-wave down the tubing and casing. Only a small fraction of wave energy on the tubing side of the packer is transmitted to the casing, the rest is reflected back by the impedance contrast from the sudden change of flow cross-section. The wellhead pulse amplitude is first attenuated by energy losses from the tubing. Coupling is provided by the tubing centralizers, casing and cement. Note that cement may cause the formation to be effectively hard around casing, thus limiting energy leakage from conversion of wellbore waves into conical waves in soft earth. More interestingly, however, the amplitude of the transmitted portion of the wellhead pulse is further attenuated by energy leakage from the casing across the perforated and fractured interval. Since the leakage occurs through perforations open to the fracture, the problem does not have axial symmetry and one needs to consider azimuthal distribution of wellbore wave motion. In addition, a large portion of the incident wave energy is reflected back at the perforations and the rest is transmitted to the fracture opening. Because of multiple reflections in the cased wellbore and fracture, the useful part of Stoneley-wave is very *weak*. It is therefore advantageous to place both the wave source and receivers downhole below packers.

Here, we summarize only a simplified model of Stoneley-wave propagation down a fluid-filled wellbore, without azimuthal dependence. We consider a vertical unpropped fluid injection fracture (Fig. 1). We idealize this fracture as a fluid-filled vertical crack of aperture $h$ lying between two elastic half-spaces bounded by the vertical planes $x=-h/2$ and $x=h/2$. Here $x$ is the horizontal axis perpendicular to the crack and $y$ is the horizontal axis parallel to it. Following Ferrazzini and Aki (1987), Tang and Cheng (1988, 1989) and Tang et al. (1991), our objective is to determine (1) the dispersion equation for normal modes trapped in the fluid filling the crack, and (2) the axial attenuation of the Stoneley-wave in the well bore.

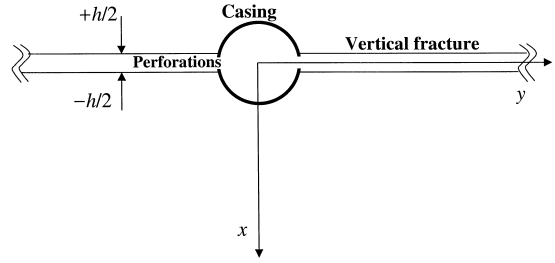


Fig. 1. Plan view of perforated casing with vertical hydrofracture. The $z$-axis is pointing downward.

### 2.1. Tang and Cheng's model of axial attenuation of wellbore waves

In a viscous fluid, a small-amplitude wave motion is governed by the usual equations of conservation of mass and momentum, linearized around the equilibrium fluid density $\rho_0$:

$$\rho_f = \rho_0 + \rho', \tag{1}$$

$\rho'$ being a small fluid density perturbation. By neglecting thermal effects in the fluid, we also simplify its equation of state:

$$p = \alpha_f^2 \rho', \tag{2}$$

where $\alpha_f$ is the acoustic velocity in the fluid.

The linearized equation of continuity is (Tang and Cheng, 1989)

$$-i\omega p + \rho_0 \alpha_f^2 \nabla \cdot \vec{v} = 0 \tag{3}$$

where $\omega$ is the angular frequency of the perturbation. Consider now a small control volume $\Delta V$ bounded by closed surface $S$ with the outside unit normal. The net volumetric flow rate from this volume can be calculated from the Gauss theorem and Eq. (3):

$$\oint_S \vec{v} \cdot \vec{n} dA = \int_{\Delta V} \nabla \cdot \vec{v} \mathrm{d}V = \int_{\Delta V} \frac{i\omega p}{\rho_0 \alpha_f^2} dV \approx \frac{i\omega p}{\rho_0 \alpha_f^2} \Delta V. \tag{4}$$

For a vertical fracture and wellbore, the control volume is a cylinder with the wellbore radius $R$ and

height $\Delta z$, Fig. 2. $S$ is the surface enclosing the cylinder, which is centered at a horizontal plane with perforations. The flux term on the left-hand-side of Eq. (4) has three parts. The first part is the net axial flux down the wellbore, $[v_z(z+\Delta z)-v_z(z)]\pi R^2$. The second part is the radial elastic flux at the wellbore wall, $v_w 2\pi R\Delta z$, where $v_w$ is the radial velocity of the wall. The third part is the oscillatory volumetric flow rate through the perforations and into the fracture, $2q_\omega/H\Delta z$, where $2q_\omega/H$ is the average oscillatory volumetric injection rate per unit length of perforated interval $H$. Substitution of these three flux components into Eq. (4), division through $\pi R^2\Delta z$, and passing to the limit as $\Delta z\to 0$ gives:

$$\frac{dv_z}{dz}+\frac{2v_w}{R}+\frac{2q_\omega/H}{\pi R^2}=\frac{i\omega p}{\rho_0\alpha_f^2} \tag{5}$$

To solve Eq. (5), we need expressions for $v_w$ and $q_w/H$. The elastic radial displacement $u_w$ of the wellbore wall is given by (Biot, 1952)

$$u_w=\frac{nI_1(nR)\,p}{\omega^2\rho_0 I_0(nR)},\quad n=\omega\sqrt{\frac{1}{c^2}-\frac{1}{\alpha_f^2}}, \tag{6}$$

where $I_0$ and $I_1$ are the modified Bessel functions of the first kind of order zero and one. The Stoneley-wave velocity is (Biot, 1952)

$$c=\frac{\alpha_f}{\sqrt{1+\dfrac{\rho_0\alpha_f^2}{G}}}, \tag{7}$$

where $G$ is the shear modulus of the formation. Multiplication of Eq. (6) by $i\omega$ gives the radial wall velocity. The low frequency limit (Tang and Cheng, 1989) of Eq. (6) is:

$$v_w\approx -i\omega\frac{Rp}{2G}. \tag{8}$$

Tang and Cheng (1989) have also obtained the oscillatory injection rate into the fracture. The opening of the hydrofracture at the wellbore allows a small fluid motion normal to the wall and into the fracture. With an oscillating pressure $p=p_0e^{-i\omega t}$ at a perforation, the fluid pressure inside the hydrofracture, averaged over the fracture aperture h, is

$$p(y)=p_0e^{i(k_y y-\omega t)} \tag{9}$$

where $y$ is the horizontal distance along the fracture (Fig. 1). The fracture-fluid wave number $k_y$ has been determined by Tang and Cheng (1989) as

$$k_y^2\tan\left(\tilde{f}\frac{h}{2}\right)+f\tilde{f}\tan\left(f\frac{h}{2}\right)=0,$$

$$f^2=\frac{\omega^2}{\alpha_f^2-\dfrac{4}{3}i\omega\upsilon}-k_y^2,$$

$$\tilde{f}^2=\frac{i\omega}{\upsilon}-k_y^2, \tag{10}$$

where $\upsilon$ is the kinematic fluid viscosity. Using Darcy's law, we obtain

$$\frac{q\omega}{H}=-C\left.\frac{\partial p}{\partial y}\right|_{y=0}=-ik_yCp, \tag{11}$$

where $C$ is the dynamic conductivity given by (Tang and Cheng, 1989)

$$C=\frac{i\omega h}{k_y^2\alpha_f^2\rho_0}. \tag{12}$$

Hence

$$\frac{q\omega}{H}==-\frac{\omega h}{k_y\alpha_f^2\rho_0}p. \tag{13}$$

Finally, the axial fluid particle velocity in the wellbore is

$$v_z=\frac{1}{i\omega\rho_0}\frac{\partial p}{\partial z}. \tag{14}$$

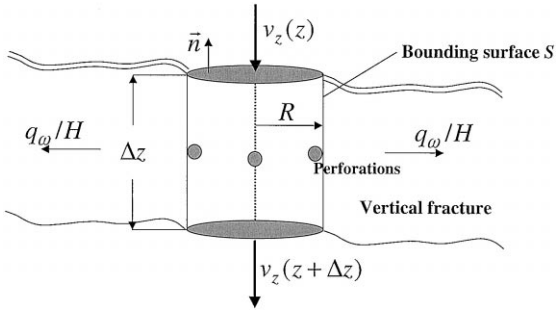


Fig. 2. Control volume for fluid mass balance.

Substituting (Eqs. (8), (13), (14) into Eq. (15), we obtain

$$\frac{\mathrm{d}^2 p}{\mathrm{d}z^2} + \omega^2\left(\frac{1}{\alpha_\mathrm{f}^2} + \frac{\rho_0}{G} + \frac{2k_y C\rho_0}{\pi R^2\omega}\right)p = 0. \qquad (15)$$

Employing Eq. (7) in the one-dimensional wave Eq. (15), we obtain the following expression for the axial wave number:

$$k_z = \frac{\omega}{c}\sqrt{1 + \frac{2k_y C\rho_0 c^2}{\pi R^2\omega}} \qquad (16)$$

The wave dispersion and attenuation in the fracture are determined by the viscosity of fracture fluid and fracture aperture. The viscous shear is limited mostly to a boundary layer with the characteristic thickness of $\delta = \sqrt{2\upsilon/\omega}$. For water $\upsilon \approx 0.01$ cm$^2$/s and $\alpha_\mathrm{f} =$ 1500 m/s. Hence, for very low frequency waves of 1–100 Hz, $\delta \approx 0.06$–$0.6$ mm, and we conclude that viscous drag in the wellbore is negligible (Shoenberg et al., 1987; Burns, 1988). In the fracture, however, viscous drag may be significant. For simplicity, we will assume that $\delta \ll h$, hence the effective fracture aperture is 10 mm or larger. Otherwise, we must determine $k_y$ numerically from Eq. (10). With this assumption

$$k_y^2 \approx \frac{\omega^2}{\alpha_\mathrm{f}^2}, \quad C \approx \frac{ih}{\omega\rho_0}, \qquad (17)$$

and Eq. (16) reduces to

$$k_z \approx \frac{\omega}{c}\sqrt{1 + \frac{2ihc^2}{\pi R^2\omega\alpha_\mathrm{f}}} \approx \frac{\omega}{c} + i\frac{ch}{\pi\alpha_\mathrm{f}R^2} \qquad (18)$$

By approximating $k_z$ with Eq. (18), a solution of Eq. (15) is

$$p(z,t) = p_0 \mathrm{e}^{i(k_z z - \omega t)} = p_0\exp\left(-\frac{chz}{\alpha_\mathrm{f}\pi R^2}\right)\exp\left[i\omega\left(\frac{z}{c} - t\right)\right] \qquad (19)$$

Eq. (19) shows that in the presence of a vertical hydrofracture, the Stoneley-wave amplitude attenuates as the wave propagates along the wellbore. The attenuation coefficient

$$\frac{ch}{\alpha_\mathrm{f}\pi R^2}, \qquad (20)$$

is proportional to the Stoneley-wave velocity and fracture aperture, and inversely proportional to the wellbore area. For the Lost Hills diatomite, a typical Young's modulus is $1.4\times10^5$ psi ($9.6\times10^8$ Pa), the Poisson's ratio is 0.34 and, consequently, the shear modulus is $G = 3.6\times10^8$ Pa. For water, $\alpha_\mathrm{f} =$ 1500 m/s and $\rho_0 = 1000$ kg/m$^3$. Substitution of these values into Eq. (7), gives $c = 560$ m/s, and $c/\alpha_\mathrm{f} = 0.37$. With the wellbore radius of 5 inches (0.127 m), the attenuation coefficient is 7.3 $h$, with $h$ expressed in m. For a perforated interval of $H = 500$ ft (152 m), and the fracture aperture of 5 mm, the wellhead pulse amplitude would be attenuated fourfold each pass of the perforated interval. Because perforations weaken coupling with the fracture, in the field we do not observe such a large attenuation.

### 2.2. Ferrazzini and Aki's model of fracture waves

A more accurate dispersion relationship for a wave in the fracture excited by a wellbore wave, was derived by Ferrazzini and Aki (1987) and adopted by Tang et al. (1991) in their later paper. Because of pressure wave propagating in the wellbore, the fluid pressure at the fracture opening near the perforations is

$$P_\mathrm{perf}(\omega,z,t) = p_0(\omega,R)\mathrm{e}^{i(k_z z - \omega t)}, \qquad (21)$$

where $p_0(\omega,R)$ is the frequency-dependent amplitude of wellbore wave at the perforations. This pressure disturbance generates another wave along the fracture, denoted by $\exp(ik_y y)$. Hence the fluid pressure in the fracture, averaged over the fracture aperture, can be written as

$$p(\omega,y,z,t) = p_0(\omega,R)\mathrm{e}^{i(k_z z + k_y y - \omega t)}. \qquad (22)$$

The wave modes in the fracture are then determined by the following dispersion equation (Ferrazzini and Aki, 1987):

$$\cot\left(\frac{hk_{\mathrm{frac}}}{2}\sqrt{\frac{v_{\mathrm{frac}}^2}{\alpha_{\mathrm{f}}^2}-1}\right) = \frac{\rho_{rock}V_{\mathrm{s}}^4\sqrt{\frac{v_{\mathrm{frac}}^2}{\alpha_{\mathrm{f}}^2}-1}}{\rho_0 v_{\mathrm{frac}}^4\sqrt{1-\frac{v_{\mathrm{frac}}^2}{V_{\mathrm{p}}^2}}}\times\left[\left(2-\frac{v_{\mathrm{frac}}^2}{V_{\mathrm{s}}^2}\right)^2 - 4\sqrt{1-\frac{v_{\mathrm{frac}}^2}{V_{\mathrm{s}}^2}}\sqrt{1-\frac{v_{\mathrm{frac}}^2}{V_{\mathrm{p}}^2}}\right], \tag{23}$$

where the $v_{\mathrm{frac}}$ is the phase velocity of the wave in the fracture and $k_{\mathrm{frac}}$ is the wave number in the fracture, which is defined as

$$k_{\mathrm{frac}} = \frac{\omega}{v_{\mathrm{frac}}} = \sqrt{k_y^2 + k_z^2}\,. \tag{24}$$

The wave modes determined by the dispersion Eq. (23), Fig. 3, have been confirmed by laboratory experiments (Tang and Cheng, 1988). Eq. (23) allows for an infinite number of normal or leaky P-wave modes, depending whether the earth is hard or soft with respect to the fracture fluid. With water in the wellbore and the fracture, diatomite is a soft formation. In particular, a fundamental mode analogous to the wellbore Stoneley mode exists for all frequencies. However, the velocity of this fundamental mode goes to zero as the frequency goes to zero while the velocity of the wellbore Stoneley mode approaches a finite limit. The fundamental mode in the fracture is most important. We assume that the wellbore pressure is uniform across the fracture aperture, which is generally small when compared with the casing perimeter. It is reasonable to assume that the wellbore pressure at the perforations will excite only the fundamental mode in the fracture, for both the rigid and elastic earth. Therefore, one can consider only the interaction of the fundamental mode in the hydrofracture with the wellbore waves. When the fundamental mode velocity is found by solving Eq. (23) numerically, the fracture-fluid wave number is obtained from Eq. (24). By differentiating Eq. (22) with respect to $y$, the pressure gradient in Eq. (11) is given by

$$\left.\frac{\partial p}{\partial y}\right|_{y=0} = ik_y p_0(\omega, R) \tag{25}$$

We now can illustrate the interaction between the fundamental fracture mode and the wellbore wave. With respect to the vertical wellbore wave, the wave front in the fracture has an angle

$$\theta = \arcsin\frac{k_y}{\sqrt{k_y^2 + k_z^2}}\,. \tag{26}$$

Fig. 3 shows that at very low frequencies, the fracture wave velocity goes to zero, while the wellbore Stoneley-wave velocity remains finite. Thus $k_y \gg k_z$ and $\theta \to \pi/2$. At low frequencies, the wellbore pressure pushes the fluid radially into the fracture, causing the strongest possible coupling between the two fluid systems. In other words, in soft rock, the hydraulic impedance test enjoys the advantage of the strongest possible coupling between the fracture and the wellbore. In addition, the wellbore wall compliance is small for both hard and soft rocks at very low frequencies (cf. Fig. 2 in Tang et al., 1991). It is

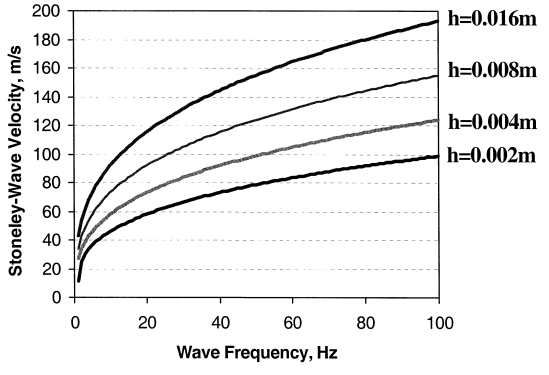


Fig. 3. Phase velocity of hydrofracture waves in soft rock vs. frequency. For the South Belridge Diatomite, typical values of the S- and P-wave velocities are $V_{\mathrm{p}} = 610$ m/s and $V_{\mathrm{p}} = 1555$ m/s, respectively. Fracture width varies from 2 mm to 1.6 cm. Note that the wave velocity is as low as 10 m/s at 1 Hz.

Table 1
Fluid flow system and its electrical equivalent
$A$ = flow cross-sectional area ($m^2$); $\rho$ = fluid density ($m^3\ s^{-1}$); $\mu$ = fluid viscosity (MPa s); $c$ = fluid compressibility ($MPa^{-1}$); $v_s$ = velocity of sound through the fluid ($m\ s^{-1}$).

| Fluid system | Electrical equivalent |
|---|---|
| Pressure (Mpa) | Voltage (V) |
| Volumetric flow rate, ($m^3\ s^{-1}$) | Electrical current (A) |
| Well elements (per unit length) | Transmission line (per unit length) |
| Fluid inertance, $\rho / A \times 10^{-6}$ | Inductance, $L$ (H) |
| Fluid capacitance, $cA = A / \rho v_s^2$ | Capacitance, $C$ (F) |
| Viscous dissipation factor, $8\ \mu\pi / A^2$ | Resistance, $R$ (W) |

therefore expected that in soft formation the effect of a fracture on the wellbore wave propagation will be more prominent at low frequencies and less significant at high frequencies, compared with the hard formation case. Hence, low-frequency hydraulic impedance testing of fracture size and state has the highest chance of success in soft rocks.

## 3. Transmission line model for the wellbore-fracture system

Pulse generated at wellhead for the impedance analysis, travels through the wellbore as a Stoneley-wave. If the wellbore radius and the fracture width are small relative to the pulse wavelength, they can be treated as analogs of electrical transmission lines. Therefore, tools for the analysis of transients in electrical transmission lines can be used to analyze the pressure transient response at the wellhead.

The flow of fluids in injection wells under applied pressure is analogous to the flow of electricity through transmission lines, with the pressure and volumetric flow rate being analogous to the voltage and electric current, respectively. Fluid inertia, energy leaks to the formation and viscous dissipation in the fracture, and energy storage due to the compressibility of fluids can be represented by their electrical counterparts, inductance, resistance and capacitance, respectively. In a lossy transmission line model, the resistance, capacitance and inductance are distributed over the line length.

Table 1 lists the components of the fluid flow system and their electrical counterparts. The well and the associated fractured reservoir can be modeled in terms of a transmission line network and lumped inductance, resistance and capacitance. The model parameters are defined completely by the relationships given in Table 1 and the geometry of the wellbore and the fracture. Fig. 4 shows the various well elements and their model equivalents. Once an electrical analog of the wellbore-fracture system is set up, the transient response of the system can be simulated with an electronic circuit simulator, e.g., SIMetrix® (Newbury Technology, 1997). As one of the built-in modules for the simulation of electronic and electrical circuit components, SIMetrix has a model of lossy electrical transmission lines. The graphical circuit building tool of SIMetrix can be used to construct a lossy transmission line network by simply interconnecting the network parts: the sources and the transmission line resistance, capacitance and inductance. Once the network is built, one

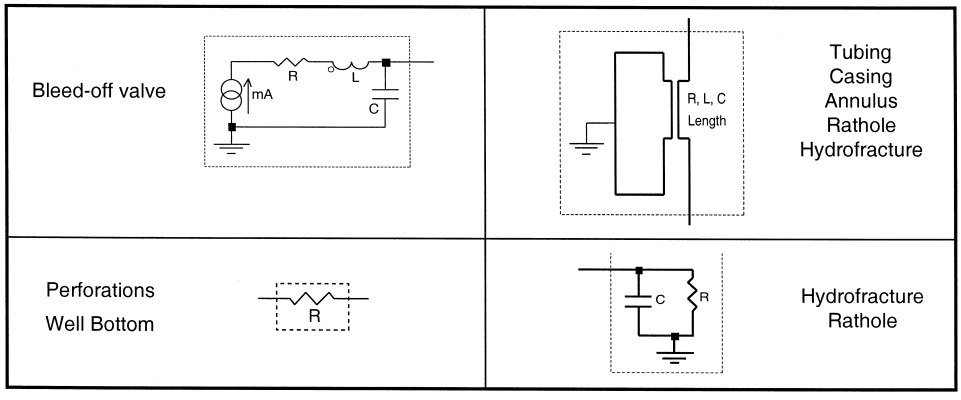


Fig. 4. Model equivalents of wellbore parts and hydrofracture.

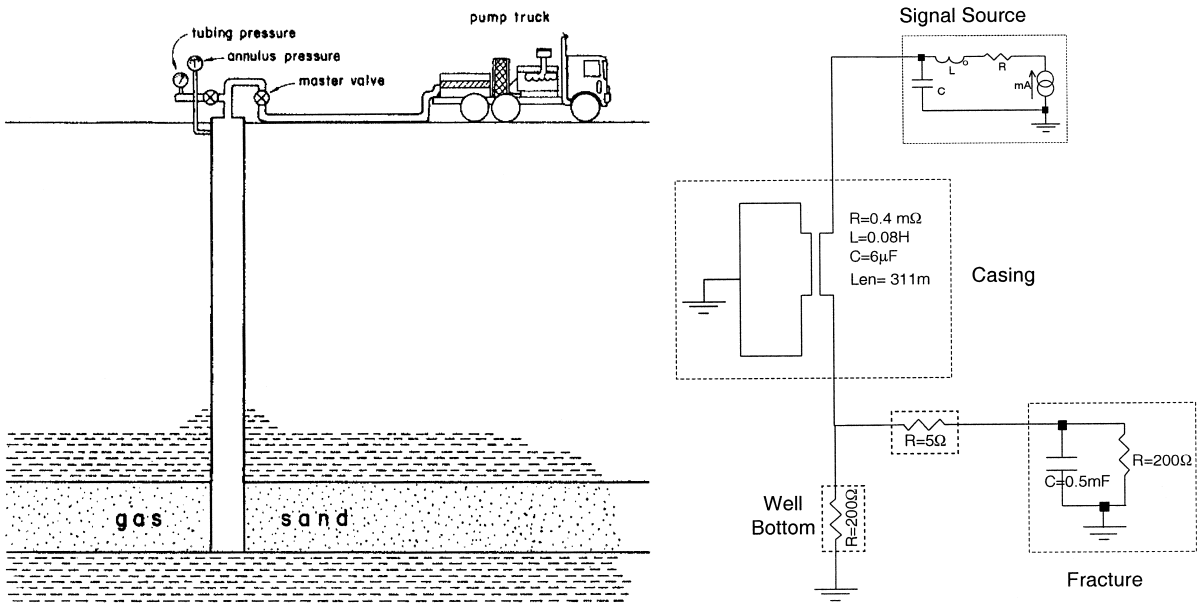


Fig. 5. Schematic of a shallow well at Mounds, OK, and its electrical analog.

can perform a transient analysis of the network and monitor the voltage and current waveforms at the desired circuit points.

### 3.1. Model verification

To validate our approach, we have analyzed several hydraulic impedance tests, both published and proprietary. Transmission line networks were constructed for the tested wellbore-hydrofracture systems, and their transient responses were simulated. The results are presented in the order of increasing system complexity.

The first example is an impedance test in a shallow well at Mounds, Oklahoma, as reported by Holzhausen and Gooch (1985). The well was cased

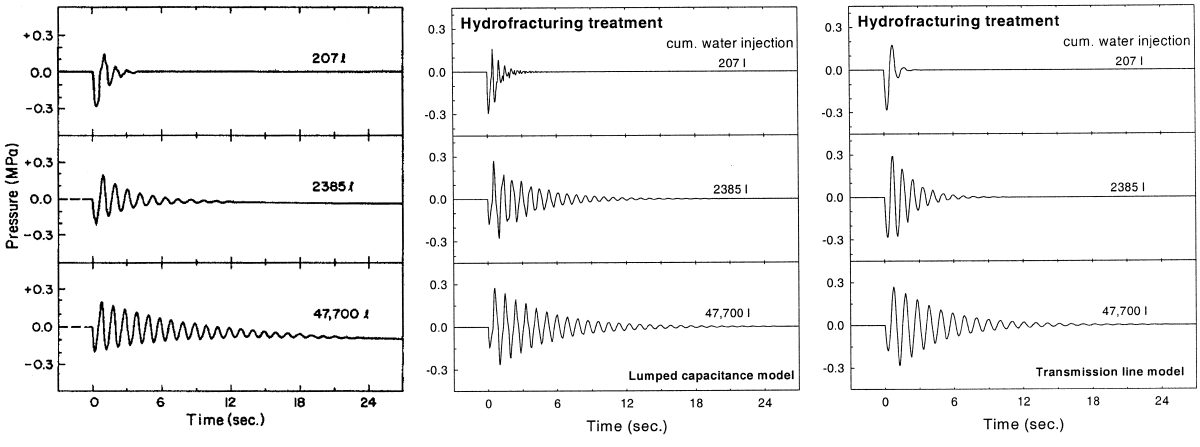


Fig. 6. Measured transient responses of the Mounds well after cumulative water injections of 207, 2385 and 47700 l, and the simulation results obtained using lumped capacitance model as well as transmission line model for the hydrofracture.

(0.126-m i.d.) to a depth of 311 m, below which there was an open-hole completion in the Skinner Sandstone. Water was injected down the casing with no tubing in the well. Fig. 5a and b show the schematic of the well and its electrical analog, respectively. While the wellbore was modeled as a lossy transmission line, the fracture was modeled both as lumped resistance and capacitance, in accordance with Holzhausen's analysis, and as a lossy transmission line.

A small hydrofracture was created and free oscillations were subsequently initiated above the fracture closure pressure after 207, 2385 and 47700 l were injected into the fracture. The transmission line model parameters for the casing were calculated from the casing geometry and the fluid properties. The lumped capacitance of the fracture was assumed proportional to the volume of water injected. When the fracture was modeled as a transmission line, the fracture dimensions were chosen to match the simulated responses, subject to the constraints imposed by the mechanical properties of the formation and the injected volumes. The measured and the simulated transient responses are shown in Fig. 6. Both the lumped capacitance and the transmission line model for the fracture result in excellent match between the experimental and the simulated response in each of the three cases. However, the transmission model is probably superior since it accounts explicitly for energy leaks from the wellbore and viscous dissipation in the fracture.

In the next example, we examine the natural response of a deep well in the presence and absence of fractures. Oscillatory wellbore pressure measurements were acquired from wellhead and downhole transducers during four in situ stress tests in a deep gas well in the Travis Peak formation of East Texas (Holzhausen et al., 1989). Fig. 7 shows the schematic of the well configuration. About 2000 l of water were first injected through perforated casing into a sandstone interval with perforations from 2732.3 to 2732.9 m. After shut-in, four free oscillations were initiated by quickly opening and closing a bleed-off valve at the wellhead, and removing no more than a few liters of water. The fracture was open during the first two oscillations and was seemingly closed during the third and fourth oscillations. We present the experimental and the simulation results for the first

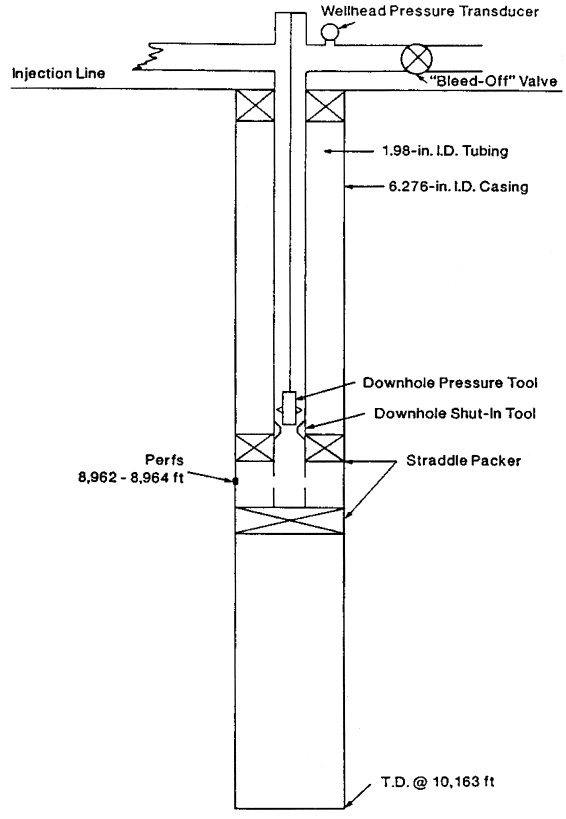


Fig. 7. Schematic of well configuration in the Travis Peak formation, Eastern Texas.

and the third water hammer events. The measured water hammers are shown Figs.8a and 9a, while the corresponding simulation results are shown in Figs. 8b and 9b. As can be seen from Fig. 8, when the first descending impulse arrives at the well bottom, it is rapidly damped by the large capacitance inherent to an open, compliant fracture. Furthermore, the initial negative impulse at the wellhead, produced by the opening and closing of the valve, is followed by a positive reflection from the bottom of the hole, indicating that the downhole reflection coefficient is negative. Hence, the fracture is open during this test. We also note that, because of the depth of the well, there is a 2-s delay in the arrival of the reflected wave at the wellhead. Thus, there is a complete temporal resolution of the traveling wave as it undergoes successive reflections. As can be seen from Fig. 8b, the transmission line network model for the system captures these features very well.

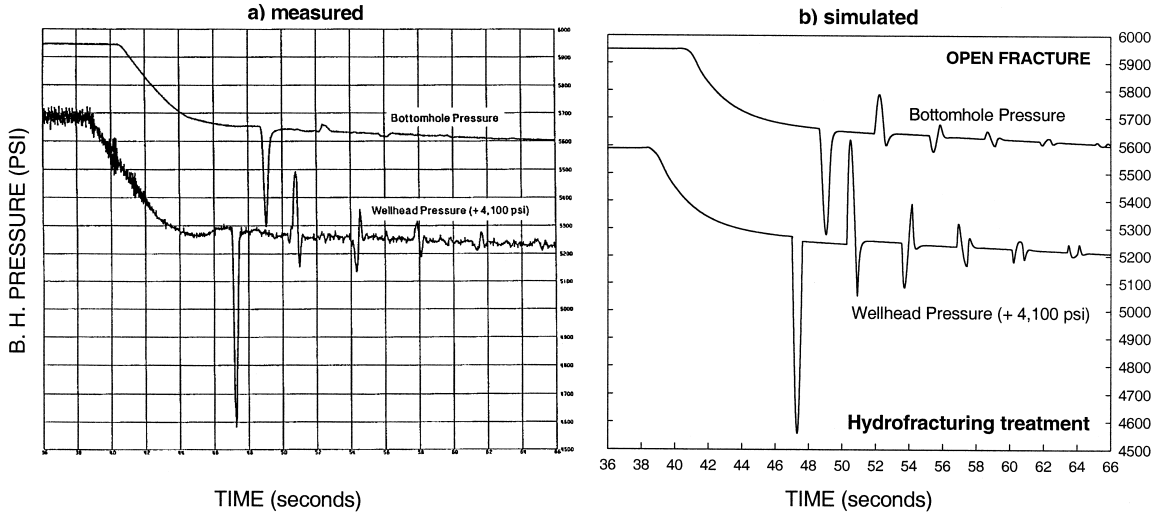


Fig. 8. The measured and simulated transient response of a deep gas well in the Travis Peak formation in the presence of open fracture.

The third impulse, which is detailed in Fig. 9, shows the resulting pressure oscillation, which lasts for several wellbore lengths. Note that the reverberating pulses, while continuing to damp, maintain a constant polarity. This suggests that the fracture is no longer compliant nor is it capable of supplying fluid to the low-pressure impulse; therefore, the fracture is closed. The simulation results are in excellent agreement with the experimental data.

The next three examples are from a waterflood in the South Belridge Diatomite, Kern County, CA (Applied Geomechanics, 1990). The following general procedure as used for each of the injection wells tested. A pressure step testing was first performed and, at the end of each step, injection was shut down and injection lines were isolated from the wellhead. Free oscillations were then initiated at the wellhead, and recorded over time. The well geometry, pressure steps and the state of fractures for each of the wells are summarized in Table 2.

In the previous example, owing to the depth of the well and its geometry, the successive reflections of the pressure pulse were temporally resolved at the wellhead. In the case of diatomite wells, unfortunately, because of the shallow well depths and closeness of reflectors, such temporal resolution of the

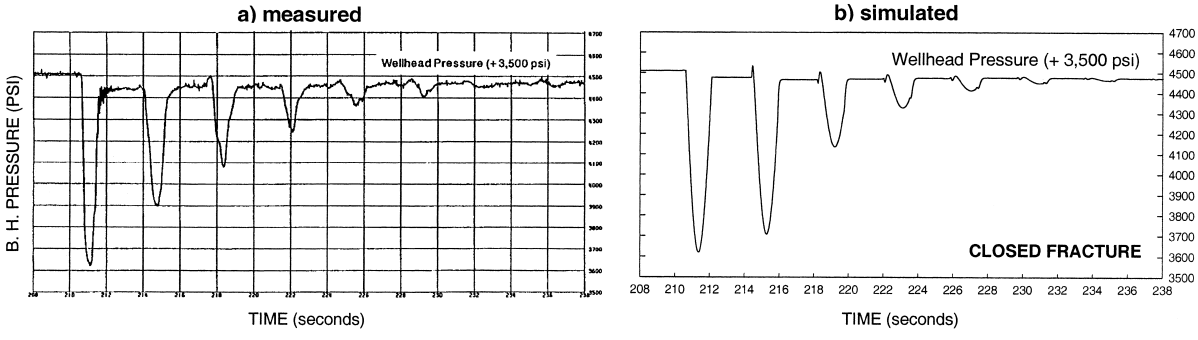


Fig. 9. The measured and simulated transient response of the deep gas well in the Travis Peak formation, in the case of closed fracture.

Table 2
Summary of well geometry, pressure steps and the fracture states for the injectors in the South Belridge Diatomite
Casing ID: 6 in. (0.15 m); central tubing ID: 2 in. (0.05 m).

| Well ID | Well geometry | Pressure step | State of fracture |
|---|---|---|---|
| 567G-33 | Tubing: 231 m<br>Interval: 95 m<br>Rathole: 58 m | 123 psi (1.79 MPa)<br>241 psi (3.50 MPa) | open<br>open |
| 552LR-33L | Tubing: 357 m<br>Interval: 114 m<br>Rathole: 27 m | 144 psi (2.09 MPa) | open |
| 534L-33 | Tubing: 200 m<br>Interval: 95 m<br>Rathole: 90 m | 93 psi (1.35 MPa)<br>100 psi (1.45 MPa) | closed<br>open/closed |
| 542L-33S | Tubing: 186 m<br>Total Interval: 143 m<br>Rathole: 6 m<br># of intervals: 2 | 115 psi (1.67 MPa)<br>181 psi (2.63 MPa) | closed<br>open |
| 531GR-33 | Tubing: 190 m<br>Total Interval: 291 m<br>Rathole: 51 m<br># of intervals: 3 | 87 psi (1.26 MPa)<br>135 psi (1.96 MPa) | closed<br>open |
| 555E-33 | Tubing: 192 m<br>Total Interval: 363 m<br>Rathole: 8 m<br># of intervals: 5 | 150 psi (2.18 MPa)<br>260 psi (3.77 MPa) | open<br>open |

reflected waves is not possible. The time-domain response of these wells to a pressure pulse, measured at the wellhead, is a superposition of successive reflections of a traveling wave. These reflections

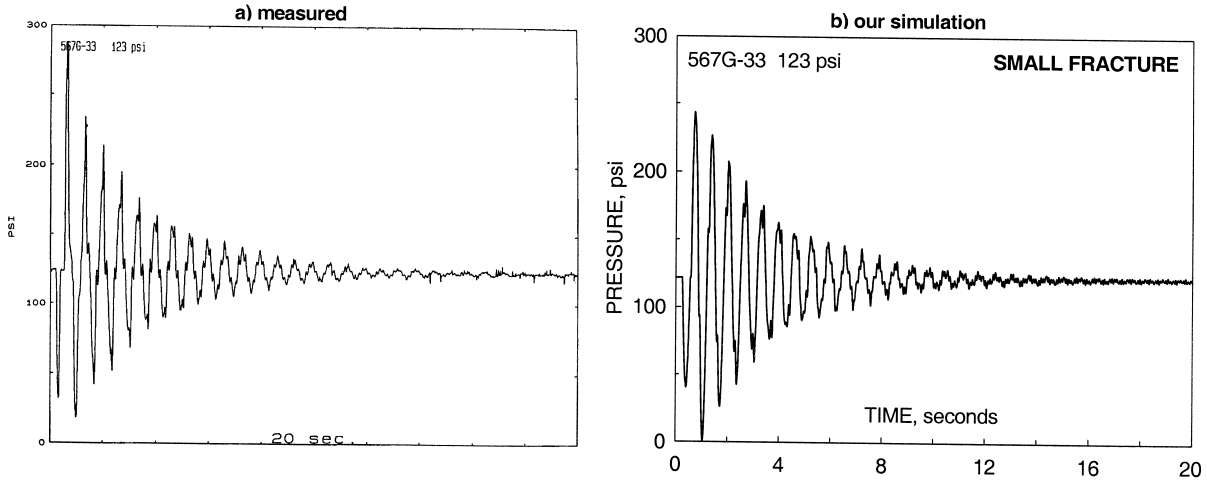


Fig. 10. The measured and simulated transient response of injection well 567G-33 in the South Belridge Diatomite waterflood, after a pressure step of 123 psi (1.79 MPa).

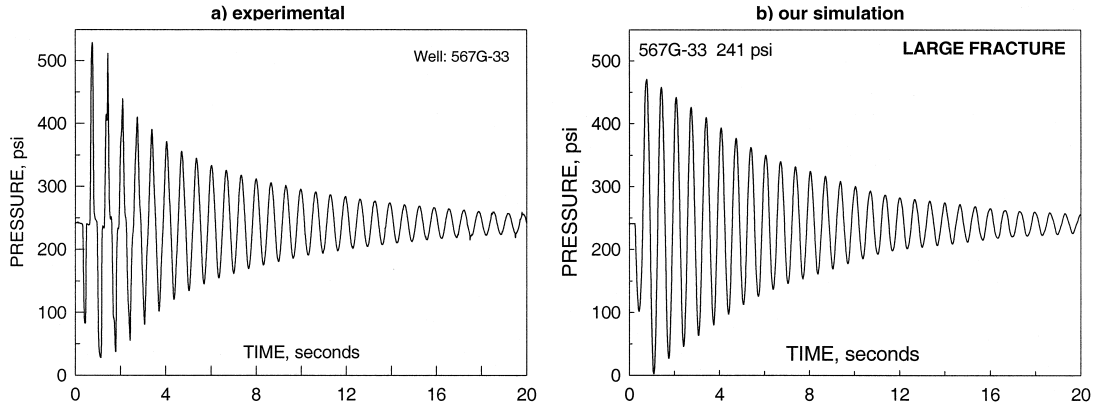


Fig. 11. Transient response of injection well 567G-33 in the South Belridge Diatomite waterflood, after a pressure step of 241 psi (3.50 MPa).

occur at the tubing tail, the well bottom, the fracture mouths for an open fracture and, possibly, from the fracture tip. Consequently, the time-domain response is rather complicated. Nevertheless, the important features, namely, the fracture location, size and state, are observable from the transient response. In all examples, the simulation results are in good agreement with the experimental data.

The first example is a shallow well (567G-33) with a 231 m tubing, one perforated interval of 95 m, followed by 58 m of unperforated casing cemented at the bottom. Step-tests were done at 123 psi (1.79 MPa) and 241 psi (3.5 MPa). In both cases, the fracture was presumably open.

Figs. 10 and 11 show the measured and simulated transient responses of well 567G-33 after pressure steps of 123 psi and 241 psi, respectively. The quick attenuation of the pressure signal during the first pressure step, indicates that the impedance mismatch between the casing and the fracture is small, and the fracture is relatively small. Experimental transient response obtained after the step-test at 123 psi was

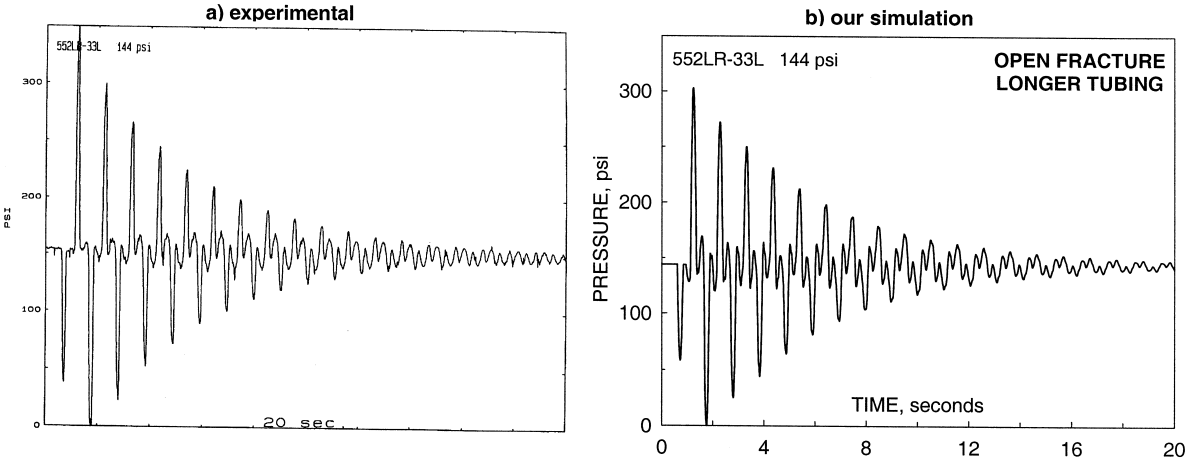


Fig. 12. Transient response of injection well 552LR-33L in the South Belridge Diatomite waterflood, after a pressure step of 144 psi (2.09 MPa).

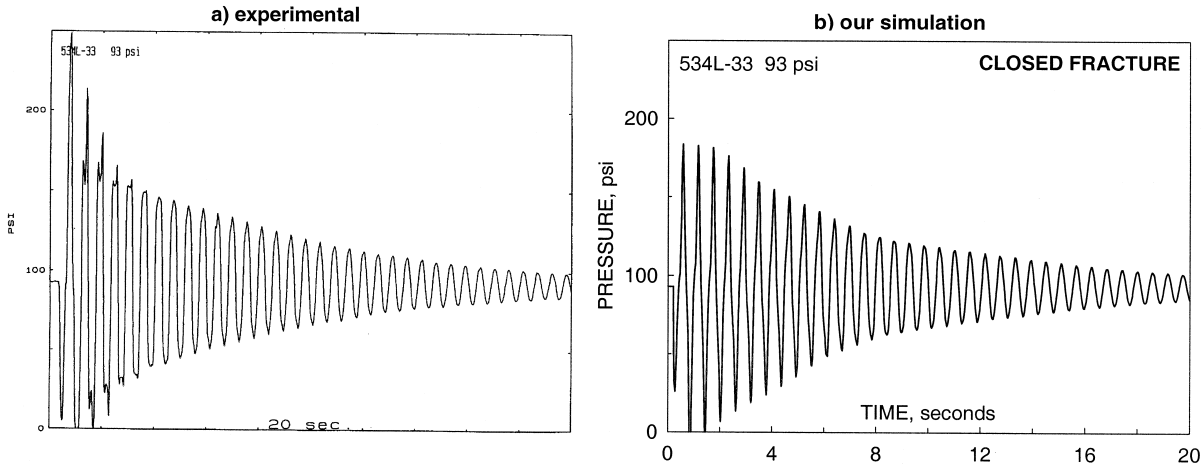


Fig. 13. Transient response of injector 534L-33 in the South Belridge Diatomite waterflood, after a pressure step of 93 psi (1.35 MPa).

matched by assuming a small fracture located near the top of the interval. On the other hand, accurate simulation of the transient response at 241 psi required a considerably larger fracture. While experimental verification of these assumptions was not possible, they are consistent with the expected behavior of the fracture.

Fig. 12 shows the transient response of well 552LR-33L, generated after a pressure step testing at 144psi (2.09 MPa). A comparison of Figs. 10 and 12 indicates that the transient responses of these two wells are significantly different after step testing at similar pressures. Simulation studies indicated that the fracture sizes were comparable in the two cases; the difference in the time-domain responses is primarily caused by the partial temporal resolution of reflected waves in 552LR-33L because of its longer tubing.

The final example is from well 534L-33, where impedance tests were carried out after step testing at pressures of 93 (1.35 MPa) and 100 psi (1.45 MPa). The transient responses for these two cases are shown

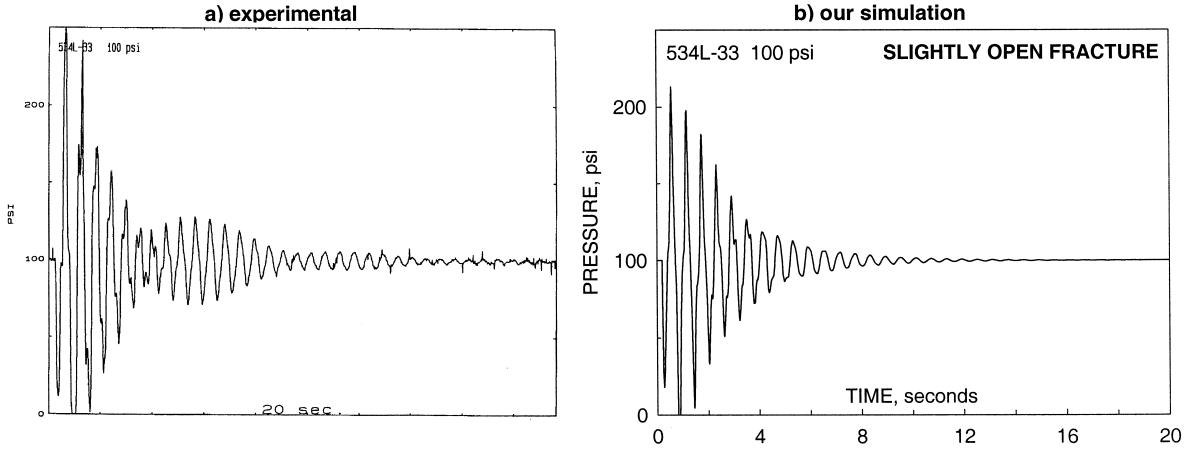


Fig. 14. Transient response of injection well 534L-33 in the South Belridge Diatomite waterflood, after a pressure step of 100 psi (1.45 MPa) (in the simulation, the fracture was assumed to be open).

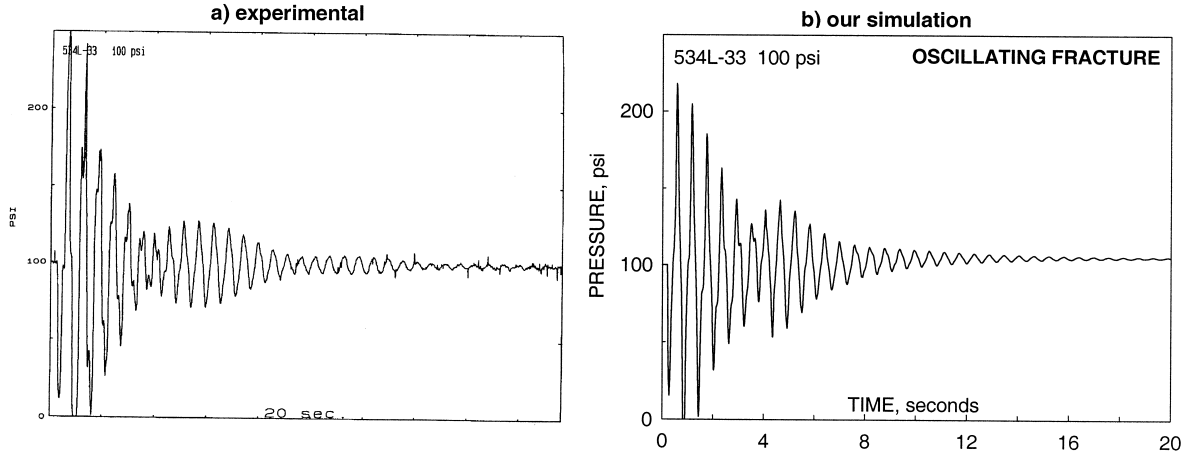


Fig. 15. Transient response of injection well 534L-33 in the South Belridge Diatomite waterflood, after a pressure step of 100 psi (1.45 MPa) (for the simulation, the fracture was assumed to be partially closed).

in Figs. 13 and 14. Fig. 13 shows a lower attenuation of the reflected waves when impedance analysis was performed after the pressure step-test at 93 psi, which suggests that the fracture was closed. The transient response of the well after a pressure step-test at 100 psi, however, shows a sharp decay of the signal with time, indicating the presence of a small fracture. Instead of a continuous decay of the signal, the transient response shows a beat-like pattern, which cannot be reproduced in our simulation with a small open fracture. To account for this discrepancy, we had to assume that the fracture closed for a short time and then reopened. This assumption is plausible because the 100-psi pressure-step is only slightly above the fracture closure pressure. A simulation, performed under this assumption, does indeed result in a beat-like pattern, similar to that obtained experimentally. The time-domain plots of the simulated and the experimental data are shown in Fig. 15.

If fractures are modeled as lumped capacitance, and the decay envelope is exponential, the slope of the logarithm the relative peak amplitude as a function of time is inversely proportional to the fracture size. For a transmission line model of a fracture, its length is obtained directly from the model. We illustrate this for several diatomite wells. For clarity of presentation, these wells are grouped according to the number of perforated intervals. The attenuation plots for one-, two-, three-, and five-interval wells are shown in Figs. 16–19, respectively.

As can be seen from these figures, at short times the pressure peaks do decay approximately exponentially. The observed nonlinearity at longer times is presumably caused by wave energy confinement in the tubing. Because of the stronger coupling between the casing and the rock than between the tubing and the rock, energy loss through the cased portion of the

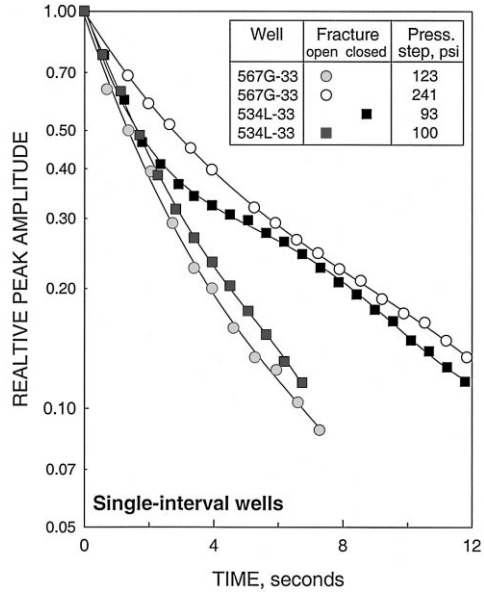


Fig. 16. The attenuation of pressure peaks during transient analysis in single-interval injection wells in the South Belridge Diatomite.

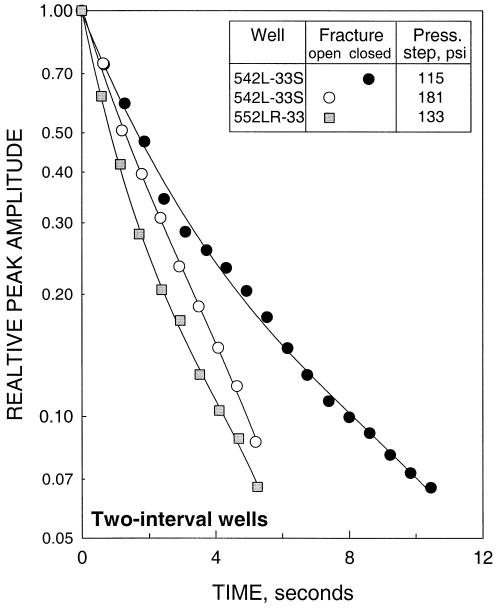


Fig. 17. The attenuation of pressure peaks during transient analysis in two-interval injection wells in the South Belridge Diatomite.

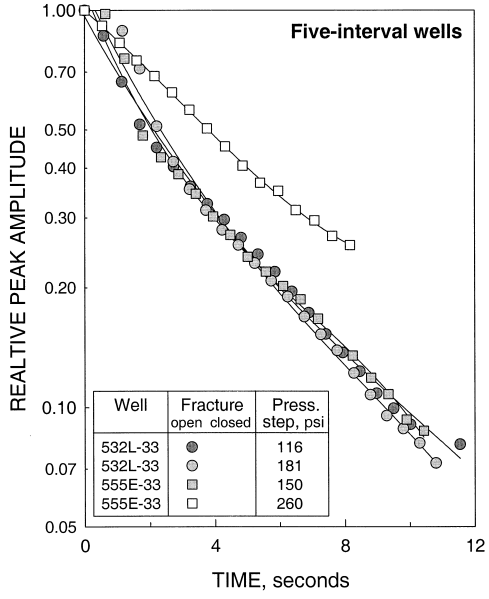


Fig. 19. The attenuation of pressure peaks during transient analysis in five-interval injection wells in the South Belridge Diatomite.

wellbore is higher than that through the tubing. Closed fractures are characterized by relatively low rate of attenuation, since no energy is dissipated in the fracture. In general, for wells of comparable depths the higher initial pressures result in lower rates of attenuation. Since higher injection pressure usually leads to larger fractures, this implies that even a simple analysis of the decay envelope may provide a relative measure of change in fracture size over time.

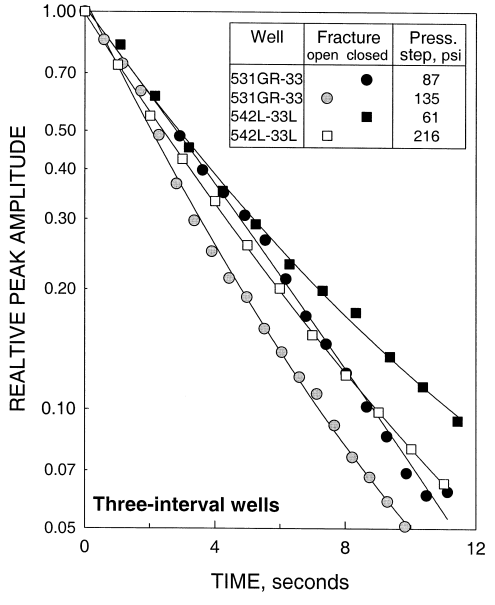


Fig. 18. The attenuation of pressure peaks during transient analysis in three-interval injection wells in the South Belridge Diatomite.

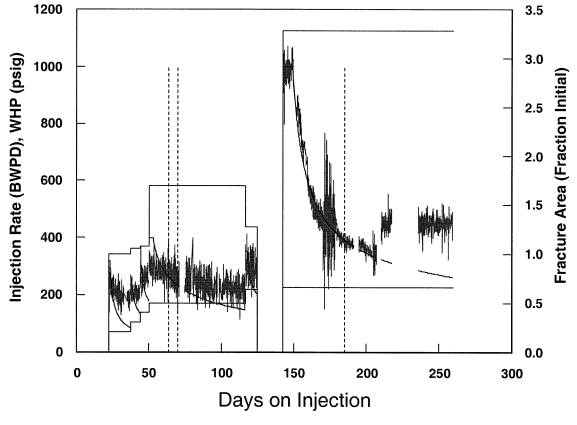


Fig. 20. Catastrophic hydrofracture extension (Patzek, 1992) in 555E-33. The vertical dotted lines denote instantaneous hydraulic impedance tests.

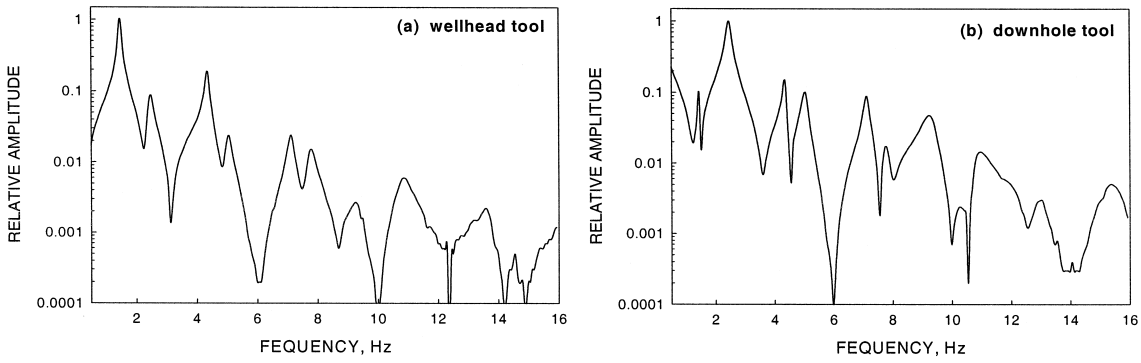


Fig. 21. Detection of signals from the fracture by a tool placed at (a) wellhead and (b) downhole.

The higher rate of energy loss through the perforated portion of casing is clearly demonstrated in Fig. 18. Two wells of nearly the same depth (532 m for 531GR-33 and 536 m for 542L-33L), but with significantly different perforated intervals (342 and 195 m, respectively) are shown. For both open and closed fractures, the attenuation rates of pressure peaks are higher in 531GR-33, with longer perforations, as compared with those in 542L-33. Thus, our ability to detect small changes in fracture size diminishes for deeper wells with longer perforations. Fig. 19 shows that the rates of attenuation of the pressure peaks during hydraulic impedance tests in 532L-33, performed after pressure step-tests at 115 and 181 psi (1.67 and 2.63 MPa), are similar. In the case of 555E-33, however, where the fracture is known to have grown by a factor of two between the transient analyses (Fig. 20), the effect of fracture size on the rate of attenuation is clearly discernible. The higher rate of attenuation of the pressure peaks during transient analysis, after a step-test at 150 psi performed prior to the catastrophic fracturing, indicates the presence of a small fracture, in accordance with the estimated fracture area.

The detection of fracture size from wellhead measurement of transient pressure response becomes more difficult as the perforated interval length increases. Therefore, a downhole tool may lead to improved resolution. Two simulations were performed. In one, the pulse source and the receiver were placed at wellhead, while in the other the transmitter-receiver pair was placed downhole. The well and the fracture geometry were identical. The normalized Fourier power spectra of the transient

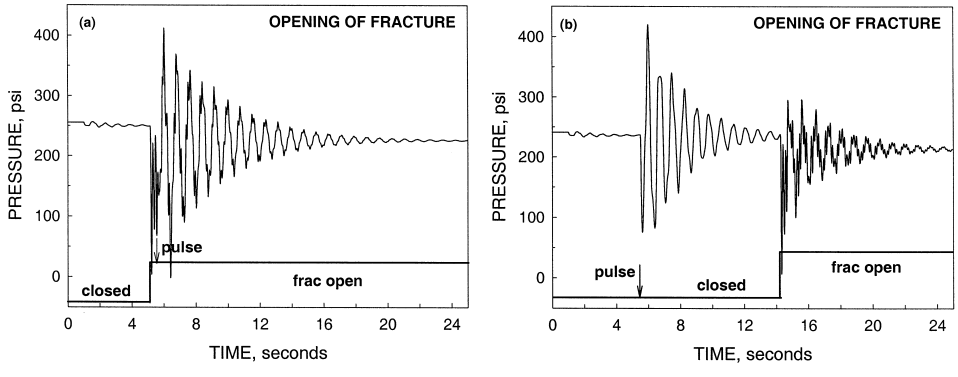


Fig. 22. Detection of a simulated fracturing event through pulsing at wellhead: a) pulse coincides with fracture opening, b) pulse occurs before fracture opening.

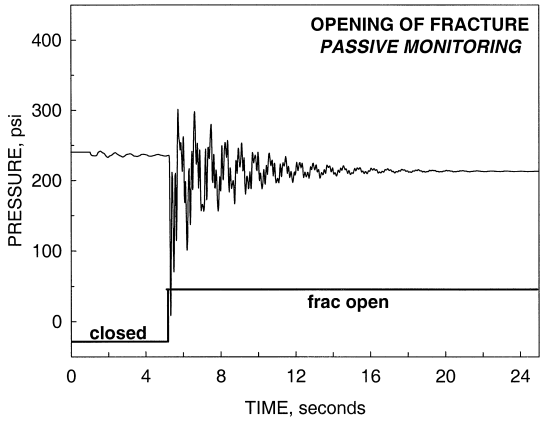


Fig. 23. Detection of a simulated fracturing event through listening at wellhead.

responses are shown in Fig. 21. It is apparent that the downhole tool results in better detection of reflections from the fracture.

Fracturing events can be detected actively, by a periodic wellhead pulsing, or passively, by listening to a pressure response. Three simulations were performed. In the first case, a pulse coincided with a fracture extension. In the second case, fracture extension occurred after the pulse was significantly attenuated. In the third, the wellhead pressure was continuously monitored to detect any pressure fluctuation from a sudden opening of a fracture. Fig. 22 illustrates the effect of a sudden fracture opening on the transient response of a pulsed well. The fracturing event creates a pressure oscillation, which is quite distinct from the natural transient response to the pulse. Even when the well is not pulsed, a sudden fracture opening creates pressure oscillations that can be detected at wellhead (Fig. 23).

## 4. Conclusions

1. A real-time ‘‘observer’’ of injection fracture state and volume is viable. The observer can be placed at wellhead or, better, below packers.
2. Very low frequency (1–100 Hz), Stoneley-waves in a fluid-filled cased wellbore interact with the fundamental wave mode in vertical hydrofracture.
3. In soft rock, the fundamental fracture wave is extremely slow: its phase velocity is about 10–100 m/s for frequencies 1–100 Hz and fracture widths of 0.2–2 cm.
4. Stoneley-wave loses energy to the fracture and energy transfer from the wellbore to the fracture opening is most efficient in soft rocks.
5. Placing the wave source and receivers beneath the injection packer provides the most efficient means of hydrofracture monitoring.
6. The wellbore-fracture systems can be modeled as a lossy transmission line network. The model parameters are completely defined by the system geometry and the fluid properties.
7. The model captures the wellbore-fracture dynamics quite accurately for a variety of well geometries.
8. A hydrofracture can be modeled either as a lumped capacitance or as a transmission line without affecting the accuracy of the simulation. However, the lossy transmission line model is superior because it allows us to account explicitly for energy leaks from the wellbore and viscous dissipation in the fracture.
9. A fracturing event can be detected by either passive or active pressure monitoring at wellhead.
10. Detection of such events will allow proper control of injection pressure during sudden fracturing and prevent uncontrolled growth of injection fractures.

## 5. Future work

Having validated the lossy transmission line model, we now can develop and deploy in the field a model-based observer of injection fractures. For computational efficiency, we need to develop a model-based inversion of the transient response data to determine fracture characteristics. Since wellbore geometry is likely to be time-invariant, the identification problem, therefore, will be reduced to the determination of fracture size only. Conversely, it is conceivable that when fracture geometry is constant, a change in well geometry and, hence, casing and tubing failure can be detected.

## 6. Notation

| | |
|---|---|
| $C$ | Dynamic conductivity |
| $G$ | Shear modulus of the formation |
| $H$ | Length of perforated interval |
| $R$ | Well radius |
| $S$ | Closed surface enclosing a control volume |
| $h$ | Fracture aperture |
| $k_y$ | Fracture fluid wave number |
| $k_z$ | Axial wave number |
| $k_{\text{frac}}$ | Wave number of the fracture |
| $p$ | Fluid pressure |
| $q_\omega$ | Oscillatory volumetric injection rate of fluid |
| $u_{\text{w}}$ | Elastic radial displacement of the wellbore wall |
| $\vec{v}$ | Fluid velocity |
| $v_{\text{w}}$ | Radial velocity of the wellbore wall |
| $v_z$ | Axial component of fluid velocity |
| $v_{\text{frac}}$ | Phase velocity of wave in the fracture |
| $z$ | Depth |
| $\Delta V$ | Control volume |
| $\Delta z$ | Height of the cylindrical control volume |
| $\alpha_{\text{f}}$ | Acoustic velocity in the fluid |
| $\delta$ | Characteristic thickness of the fluid boundary layer |
| $\upsilon$ | Kinematic fluid viscosity |
| $\omega$ | Angular frequency of fluid density perturbation |
| $\rho_0$ | Equilibrium fluid density |
| $\rho'$ | Small fluid density perturbation |

## Acknowledgements

The financial support was provided by the Assistant Secretary for Fossil Energy under the DOE Advanced Computational Technology Initiative (ACTI) contract DE-AC03-76FS00098 to the Lawrence Berkeley National Laboratory of the University of California. Partial support was provided by CalResources and Chevron Petroleum Technology Company, as gifts to U.C. Oil Consortium. We thank Aera Energy, LLC., for releasing the hydraulic impedance test data for the South Belridge Diatomite. Finally, we thank Prof. J.W. Rector for reviewing the manuscript and valuable comments.

## References

Applied Geomechanics, 1990. Results of Hydraulic Impedance Testing on Water Injection Wells in the Belridge Field, Kern, CA. AGI Report No. A-90-1004, USA.

Ashour, A.A., Yew, C.H., 1996. A study of the fracture impedance method. 47th Annual CIM Petroleum Society Technical Meeting, Calgary, Canada, 13 pp.

Biot, M.A., 1952. Propagation of elastic waves in a cylindrical bore containing a fluid. J. Appl. Phys. 53, 977–1005.

Burns, D.R., 1988. Viscous fluid effects on guided wave propagation in a borehole. J. Acoust. Soc. Am. 82 (2), 463–469.

De, G.S., Winterstein, D.F., Johnson, S.J., Higgs, W.G., Xiao, H., 1997. SPE 37773, Predicting natural or induced fracture azimuths from shear-wave anisotropy. SPE Middle East Show and Conference, Manama, Bahrain, March.

Ferrazzini, V., Aki, K., 1987. Slow waves trapped in a fluid-filled crack: implication for volcanic tremor. J. Geophys. Res. 92, 9215–9233.

Holzhausen, G.R., Branagan, P., Egan, H., Wilmer, R., 1989. Fracture closure pressures from free-oscillation measurements during stress testing in complex reservoirs. Int. J. Mechanical Mining Science and Geomechanical Abstracts 26 (6), 533–540.

Holzhausen, G.R., Egan, H.N., 1986. Fracture diagnostics in East Texas and Western Colorado using the hydraulic-impedance method. Unconventional Gas Technology Symposium of the Society of Petroleum Engineers, Louisville, Kentucky, USA, 97–108.

Holzhausen, G.R., Gooch, R.P., 1985. Impedance of hydraulic fractures: its measurement and use for estimating fracture closure pressure and dimensions. SPE/DOE 1985 Low Permeability Gas Reservoirs, Denver, CO, USA, 411–422.

Ilderton, D., Patzek, T.W., Rector, J.W., Vinegar, H.J., 1996. Microseismic imaging of hydrofractures in the Diatomite. SPE Formation Evaluation, March 46–54.

Newbury Technology, 1997. SIMetrix Analogue Simulator. Thatcham, UK.

Paige, R.W., Murray, L.R., Roberts, J.D.M., 1995. Field applications of hydraulic impedance testing for fracture measurement. SPE Production and Facilities, February: 7–12.

Patzek, T.W., 1992. Surveillence of South Belridge Diatomite. SPE Western Regional Meeting, Bakersfield, CA, USA, 171–184.

Patzek, T.W., Silin, D.B., 1998. SPE 39698, Control of fluid injection into a low-permeability rock — 1. Hydrofracture growth. SPE/DOE Improved Oil Recovery Symposium, Tulsa, OK, USA.

Shoenberg, M., Sen, P.N., White, J.E., 1987. Attenuation of acoustic modes due to viscous drag at the borehole wall. Geophysics 52 (11), 1566–1569.

Tang, X.M., Cheng, C.H., 1988. Wave propagation in a fluid-filled fracture — an experimental study. Geophys. Res. Lett. 15, 1463–1466.

Tang, X.M., Cheng, C.H., 1989. A dynamic model for fluid flow in open borehole fractures. J. Geophys. Res. 94, 7567–7576.

Tang, X.M., Cheng, C.H., Toksoz, M.N., 1991. Stoneley-wave propagation in a fluid-filled borehole with a vertical fracture. Geophysics 56 (4), 447–460.

Vinegar, H.J., Wills, P.B., De Martini, D.C., Shlyapobersky, J., Deeg, W.F.J., Adair, R.G., Woerpel, J.C., Fix, J.E., Sorrells, G.G., 1992. Active and passive seismic imaging of a hydraulic fracture in the Diatomite. J. Petrol. Technol. 44 (1), 28–77.

Winterstein, D., 1992. How shear-wave properties relate to rock fractures: simple cases. Geophysics: the Leading Edge of Exploration, September: 21–28.

Wylie, E.B., Streeter, V.L., 1978. Fluid Transients. First Edition McGraw-Hill, New York, USA.